Supporting Information

Unveiling the Role of Surface P-O Group in P-doped Co_3O_4 for Electrocatalytic Oxygen Evolution by On-chip Micro-device

Xunbiao Zhou[1], Xiaobin Liao[2], Xuelei Pan[1], Mengyu Yan[3], Liang He[1], Peijie Wu[1], Yan Zhao[2*], Wen Luo[1,4*], Liqiang Mai[1,5]*

[1]State Key Laboratory of Advanced Technology for Materials Synthesis and Processing, Wuhan University of Technology, Wuhan 430070, China

[2]State Key Laboratory of Silicate Materials for Architectures, International School of Materials Science and Engineering, Wuhan University of Technology, Wuhan 430070, China

[3]Materials Science and Engineering Department, University of Washington, Seattle, WA 98195-2120, USA.

[4]Department of Physics, School of Science, Wuhan University of Technology, Wuhan 430070, China

[5]Foshan Xianhu Laboratory of the Advanced Energy Science and Technology Guangdong Laboratory, Foshan 528200, Guangdong, China

*E-mail: luowen_1991@whut.edu.cn; yan2000@whut.edu.cn; mlq518@whut.edu.cn

Experimental Section

***Ex-situ* Raman spectra measurement.** The Raman spectra were obtained with He/Ne laser of λ = 532 nm. The CV was carried out by a CHI 760E electrochemical workstation at a scan rate of 50 mV s^{-1}. During the electrochemical cycle, the P_1-Co_3O_4 thin-film on SiO_2 substrate served as work electrode and immersed in 1 M KOH electrolyte. A platinum wire electrode and Hg/HgO (1M KOH, aqueous) served as counter and reference electrodes, respectively.

Activation energy measurement. The temperature-dependent linear sweep voltammetry (LSV) plots measurements were carried out using synthesized large-size Co_3O_4 or P-doped Co_3O_4 (P-Co_3O_4) thin-films on Au substrates as working electrode, and immersed in 1 M KOH electrolyte. The synthesis process of working electrode was similar to that shown in Figure S1, except that the 150 nm thick Au film was deposited on the silicon wafer beforehand as conductive substrate to ensure the necessary charge transport. A platinum sheet electrode and Hg/HgO (1M KOH, aqueous) served as counter and reference electrodes, respectively. Before activation energy measurement, both Co_3O_4 and P-Co_3O_4 thin-films experienced electrochemical activation process until the cyclic voltammetry (CV) curves were stable. Thus, the P_1-Co_3O_4 was converted into P'_1-Co_3O_4. A water bath was used for temperature control from 20 to 60 °C. The used electrochemical workstation is Autolab PGSTAT 302N. The actual temperatures of electrolyte were measured by a thermometer. The OER activation energy (E_a) was calculated by the Arrhenius relationship[1]:

$$\frac{\partial \log i_k}{\partial T^{-1}} = -\frac{E_a}{2.3R}$$

where i_k is the kinetic current, T is the absolute temperature, and R is the universal gas constant.

OER activity measurement of the microdevices. The device was placed on a probe station (Lake shore, PPTX). The OER performance was measured with a three-electrode configuration using an electrochemical workstation (Autolab PGSTAT 302N). The individual thin-films, including Co_3O_4, P_0-Co_3O_4 and P_1-Co_3O_4, were used as working electrode and immersed in 1 M KOH electrolyte. Notably, the P_1-Co_3O_4 thin-films were converted into P'_1-Co_3O_4 by 50 electrochemical CV cycles in the range of potential between 0 and 0.75 V vs Hg/HgO. A platinum wire electrode and Hg/HgO (1M KOH, aqueous) served as counter and reference electrodes, respectively. The electrochemical potentials were converted to the RHE scale by following equation: E (RHE) = E (Hg/HgO) + 0.9029 V. The CV experiments at a scan rate of 50 mV s^{-1} and linear-sweep voltammograms (LSV) at a scan rate of 5 mV s^{-1} were performed at 25 °C. The catalyst was cycled until the CV curves were stable, and then the OER performance was obtained by LSV testing. The electrochemical impedance spectra (EIS) were recorded at 1.6 V vs. RHE from 100000 to 0.01 Hz.

ECSA calculation. The electrochemical surface areas (ECSAs) of the catalysts were

estimated by CV experiments. CVs were performed in the potential range from 0.15 to 0.25 V (vs Hg/HgO) at varying rates from 10 to 50 mV s^{-1} in 1.0 M KOH.

Conductance calculation. The electric conductance of the thin-films was calculated by the following equation:

$$G = |\frac{\Delta I}{\Delta V}|$$

Where △V is the voltage range between -0.1 V and 0.1 V (constant value 0.2 V), and △I is the current difference between -0.1 V and 0.1 V voltage range. To note here, the surface area and thickness of all fabricated devices are almost the same (area 150 μm*150 μm, thickness 44~51 nm), thus we can normalize and compare the conductance of difference samples.

***In situ I-V* measurement.** The probe station and semiconductor device analyzer were employed to realize the *in situ* electrical measurement. Two work electrodes (WE1 and WE2), the counter electrode and the reference electrode were connected to four standard source–measure unit channels of probe station. At the electrochemical process, the electrical signal of individual thin-films was recorded in semiconductor device analyzer by connecting the WE1 and WE2 with a tiny bias voltage (△V = 1 mV).

$$\text{The real-time resistance } (R_{in\ situ}) = |\frac{\Delta V * S}{\Delta I}|$$

Where △V is the constant potential difference (1 mV) between two work electrodes, and △I is the current difference between two work electrodes. S is the surface area of thin-films between WE1 and WE2.

Computation details. Ab initio calculations were performed with the help of Vienna Ab-initio Simulation Package. Perdew-Burke-Ernzerhof (PBE) generalized gradient approximation (GGA) was carried out to examine the electronic exchange-correlation function. The energy cutoff for the plane-wave basis expansion was chosen to 520 eV. An energy difference of 1.0×10^{-5} eV/atom was set to obtain accurate electronic ground-state calculation. The maximum force tolerance was set to 0.02 eV/Å for structural optimization. The k-points for Brillioun zone were selected by Monkhorts-Pack method and set to 3×3×1.

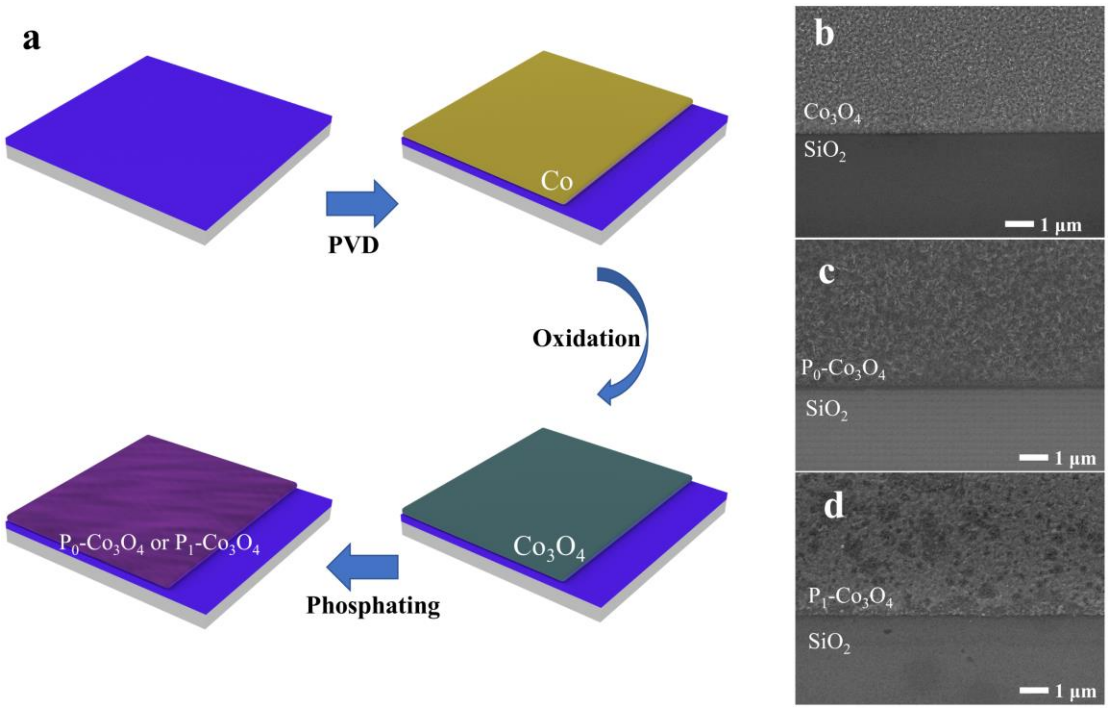

Supplementary Figure 1: Scheme illustration of the synthetic process of Co_3O_4, P_0-Co_3O_4 and P_1-Co_3O_4 thin-films **(a-d)**, and corresponding scanning electron microscopy (SEM) images **(e-g)**.

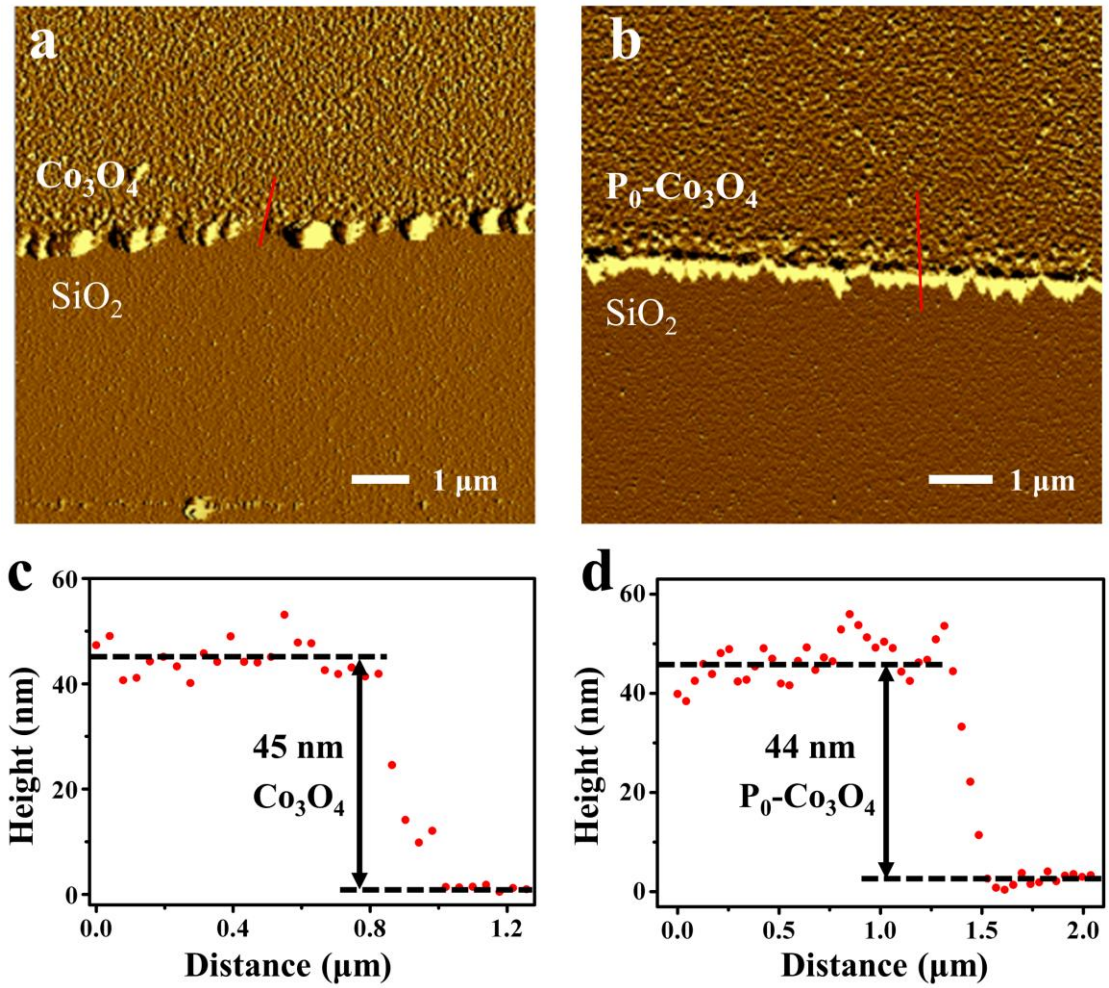

Supplementary Figure 2: The AFM images of Co_3O_4 **(a)**, and P_0-Co_3O_4 **(b)**, and the corresponding height line profiles drawn across the Co_3O_4 **(c)** and P_0-Co_3O_4 **(d)** thin-films along red lines.

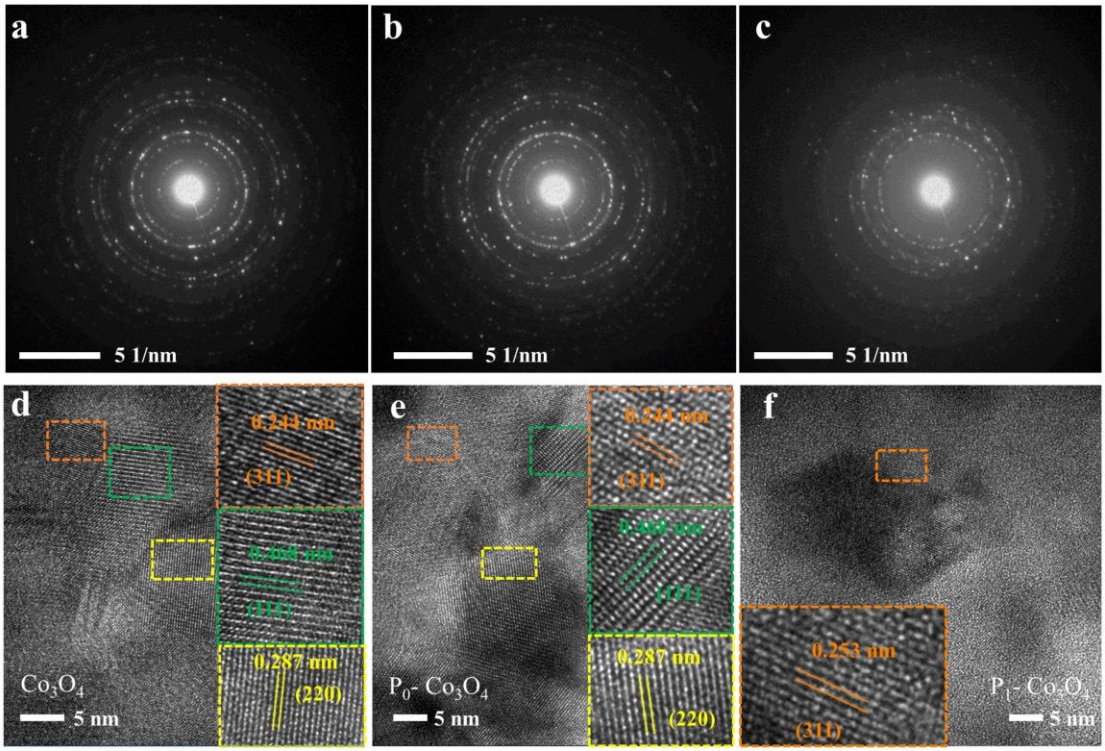

Supplementary Figure 3: SAED patterns of Co_3O_4 **(a)**, P_0-Co_3O_4 **(b)** and P_1-Co_3O_4 **(c)**, and the corresponding high-resolution transmission electron microscopy (HRTEM) images **(d-f)**.

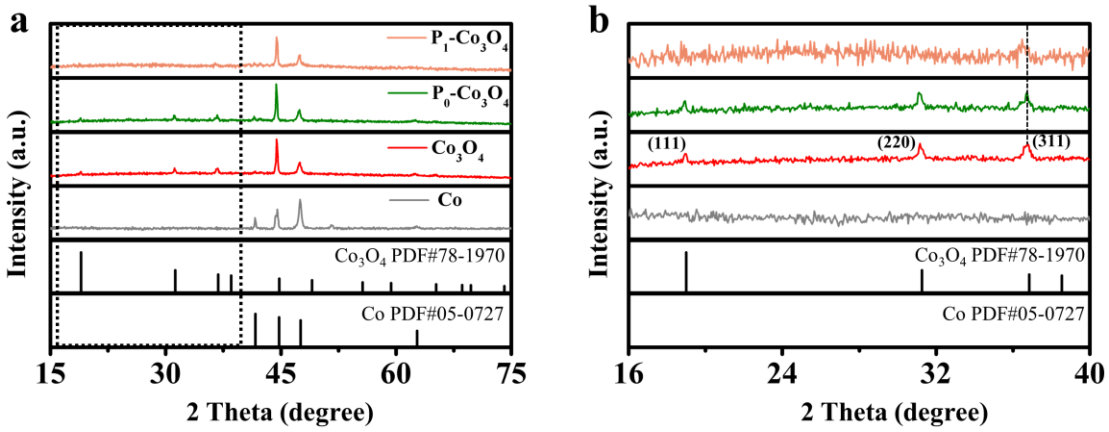

Supplementary Figure 4: The XRD pattern of Co, Co_3O_4, P_0-Co_3O_4 and P_1-Co_3O_4 in their bulk states. The peaks at 44.76 and 47.57 degree in **(a)** may be affected by Co foil. To exclude the influence of cobalt foil, local pattern (16-40 degree) were extracted for analysis, as shown in **(b)**. For P_1-Co_3O_4, the negative shift of (311) facet may imply the doping of lattice phosphorus.[2]

Note: To achieve XRD characterization, we used Co foil (purity 99.99%) as cobalt source and carry out the oxidation process at 450 °C for 40 min to obtain bulk Co_3O_4 on Co foil. And the same phosphating process was carried out at 270 and 330 °C, respectively, to obtain the bulk P_0-Co_3O_4 and P_1-Co_3O_4.

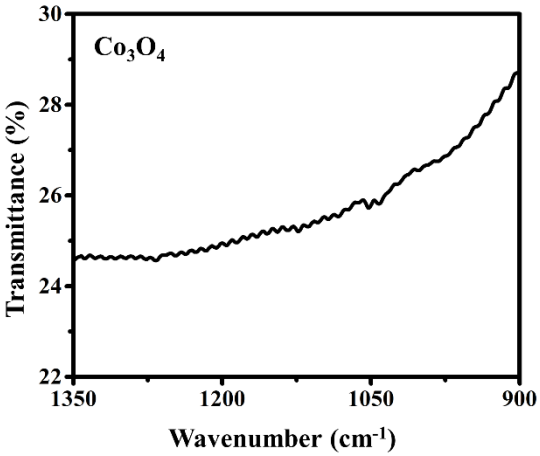

Supplementary Figure 5: The FTIR of purchased standard Co_3O_4 sample (purity 99.99%).

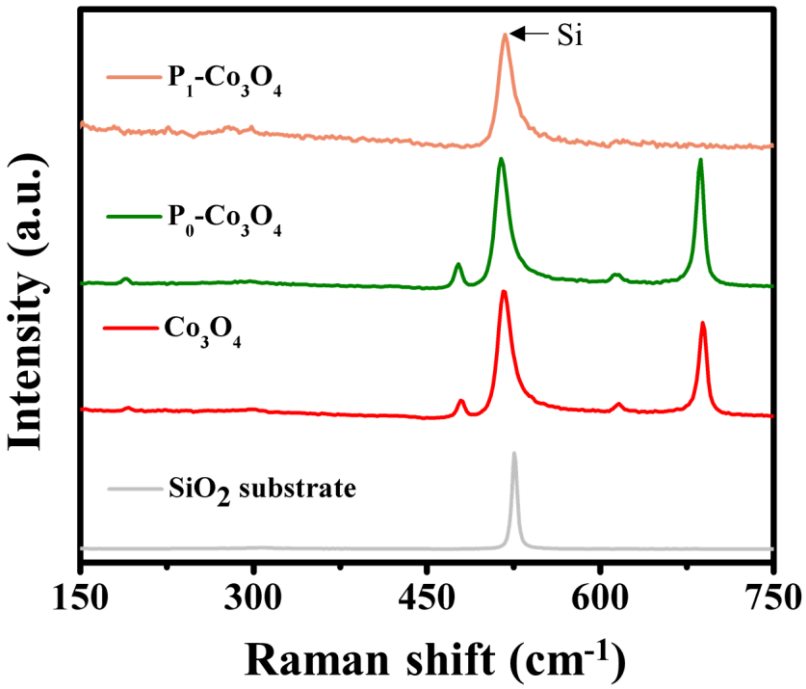

Supplementary Figure 6: Raman spectra of Co_3O_4, P_0-Co_3O_4 and P_1-Co_3O_4 thin-films on silicon wafer with 300 nm SiO_2 dielectric layer.

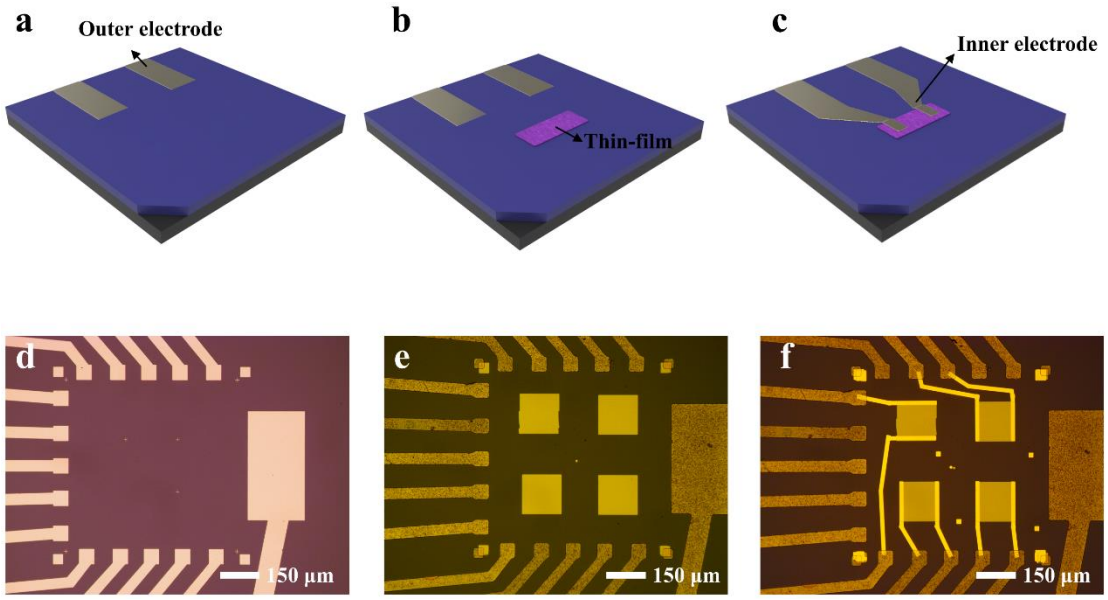

Supplementary Figure 7: The microfabrication of two-terminal thin-film devices. **(a-c)** The schematic diagram of the fabricated process. **(d-f)** The corresponding optical images of the fabricated process.

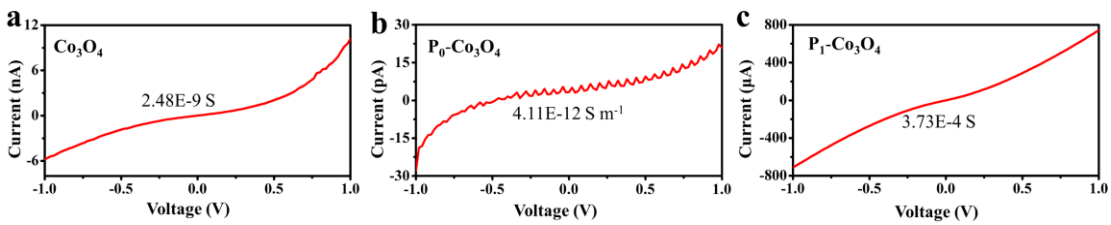

Supplementary Figure 8: The *I-V* curves of the Co_3O_4, P_0-Co_3O_4 and P_1-Co_3O_4 thin-films.

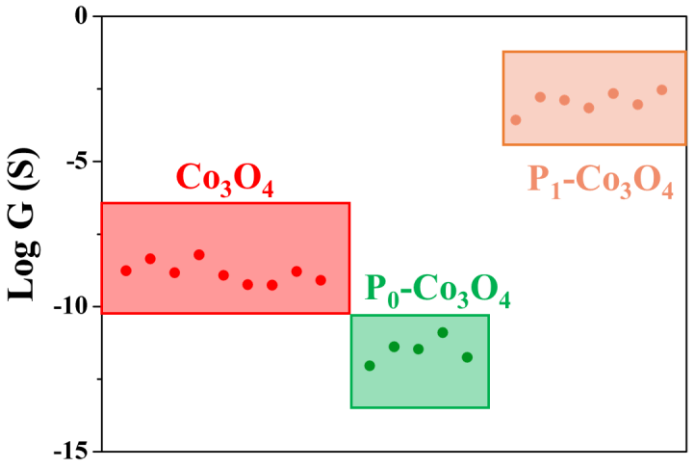

Supplementary Figure 9: Electric conductance statistical distribution diagram of Co_3O_4, P_0-Co_3O_4 and P_1-Co_3O_4.

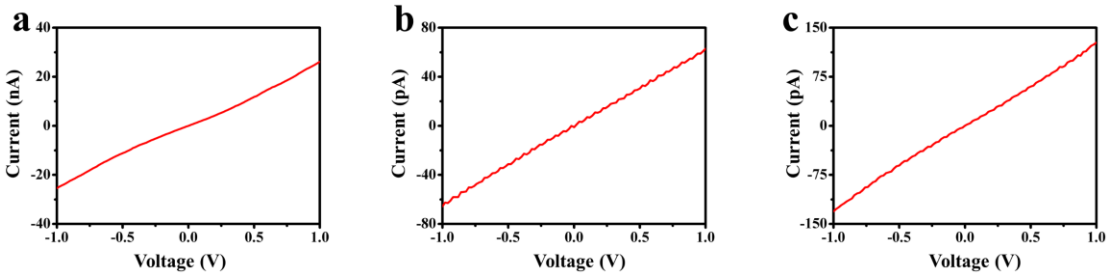

Supplementary Figure 10: The I-V curves of Co_3O_4 without annealing(a), Co_3O_4 with 270 ℃ annealing (b) and Co_3O_4 with 330 ℃ annealing (c).

Note: The annealing process was carried out in the tube furnace for 120 min under nitrogen gas atmosphere, only without NaH_2PO_2 added.

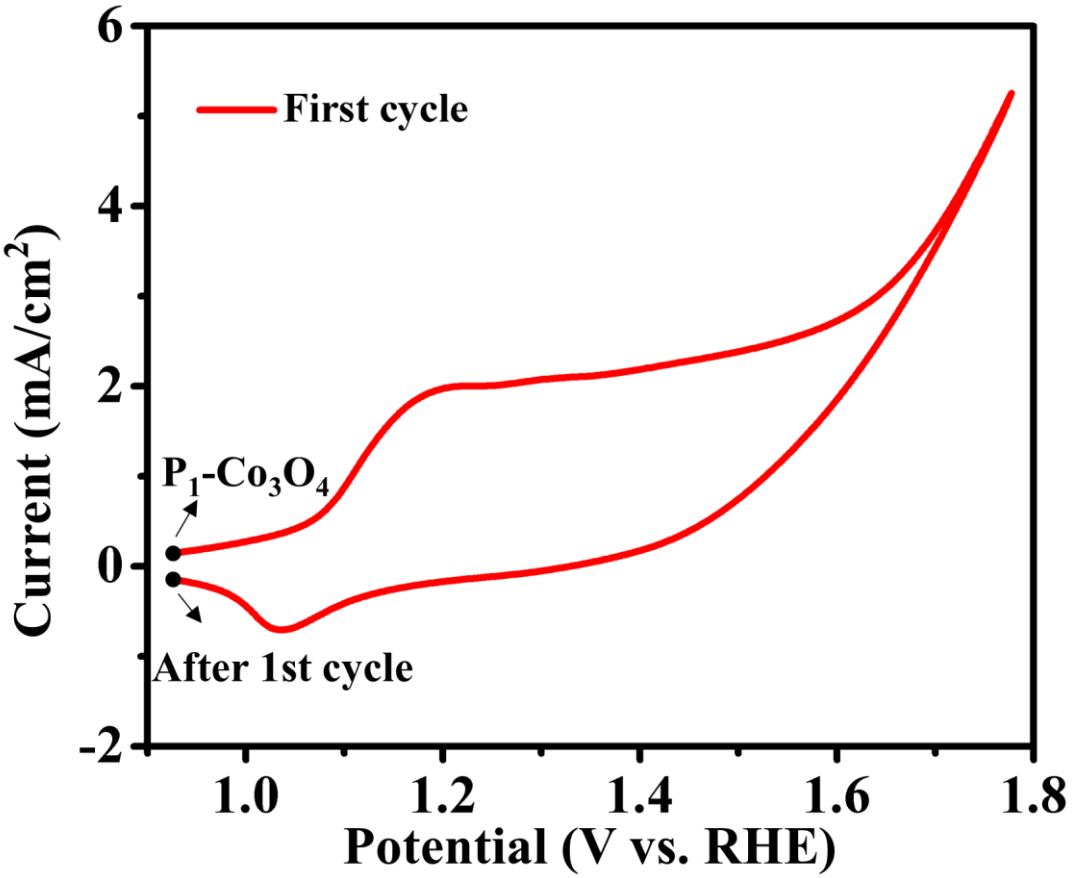

Supplementary Figure 11: the first electrochemical cycle of P_1-Co_3O_4 for Raman testing.

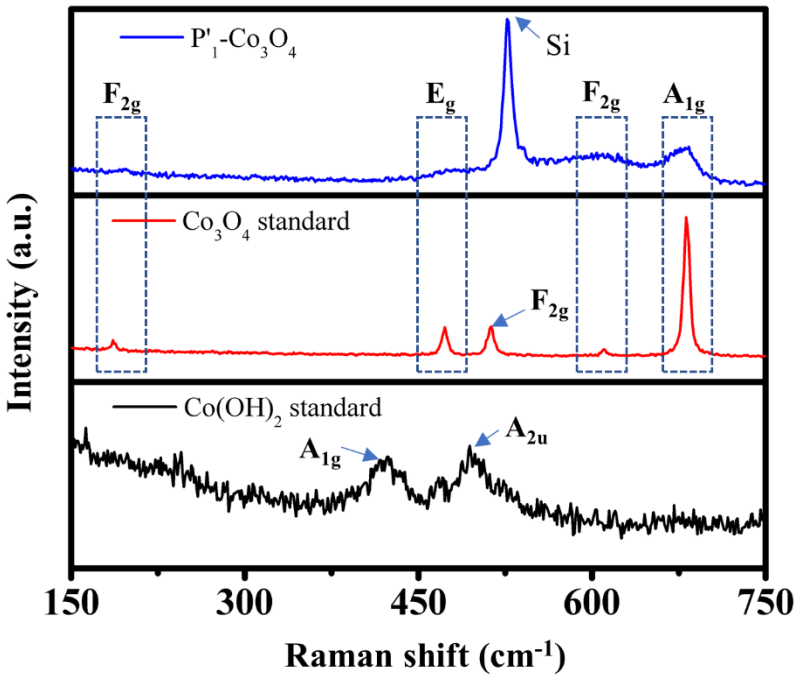

Supplementary Figure 12: Raman spectra of P'_1-Co_3O_4, standard Co_3O_4 and standard $Co(OH)_2$.

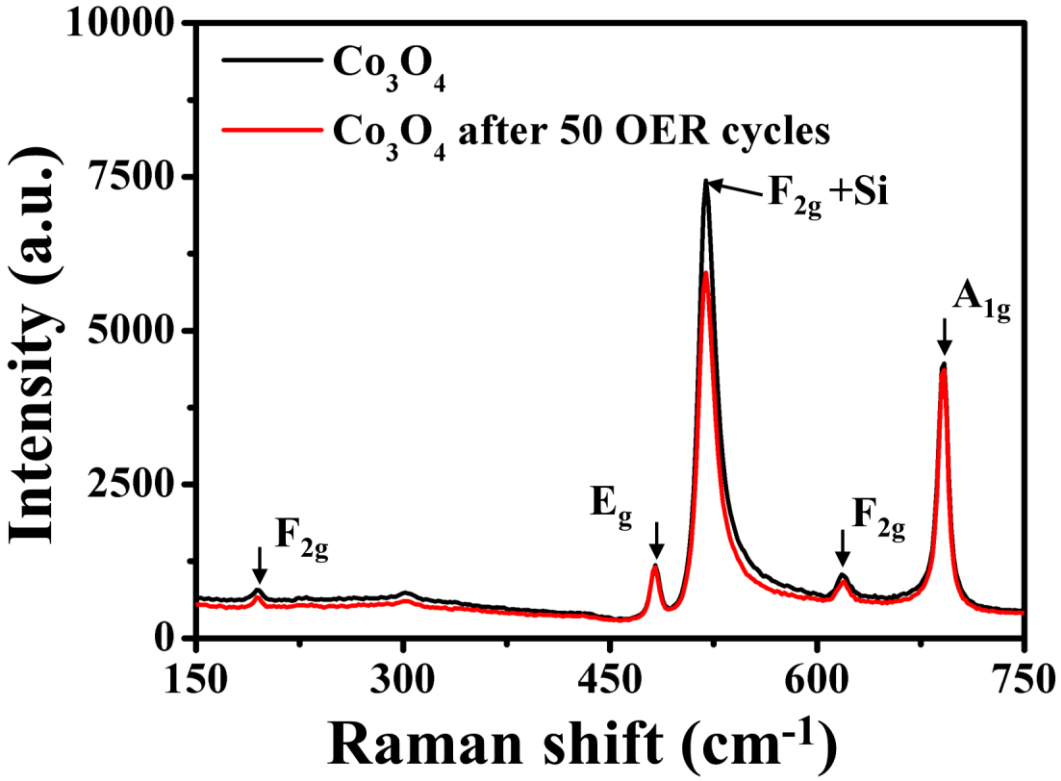

Supplementary Figure 13: Raman spectra of Co_3O_4 thin-films before and after 50 electrochemical cycles. The Raman peak at 520 cm^{-1} is related to both Co_3O_4 thin-films and SiO_2 substrate.

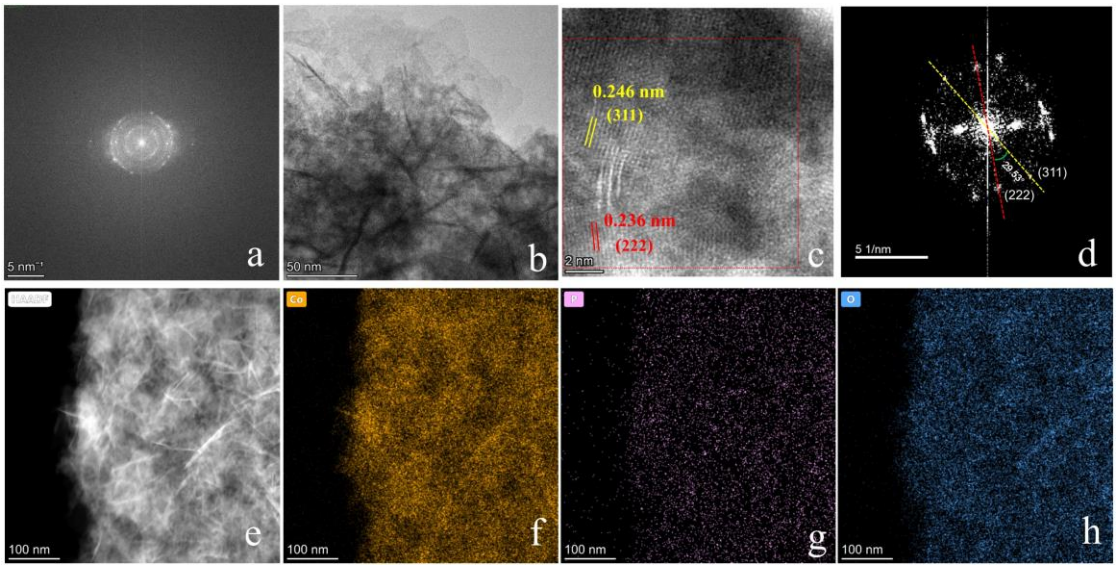

Supplementary Figure 14: The SAED pattern (a), HRTEM images (b), HAADF-STEM image (c), and the corresponding fast Fourier transform (FFT) pattern (d), which is obtained from the region inside the red dotted line in (c). (e-h) the corresponding elemental mappings of P'$_1$-Co_3O_4 thin-film.

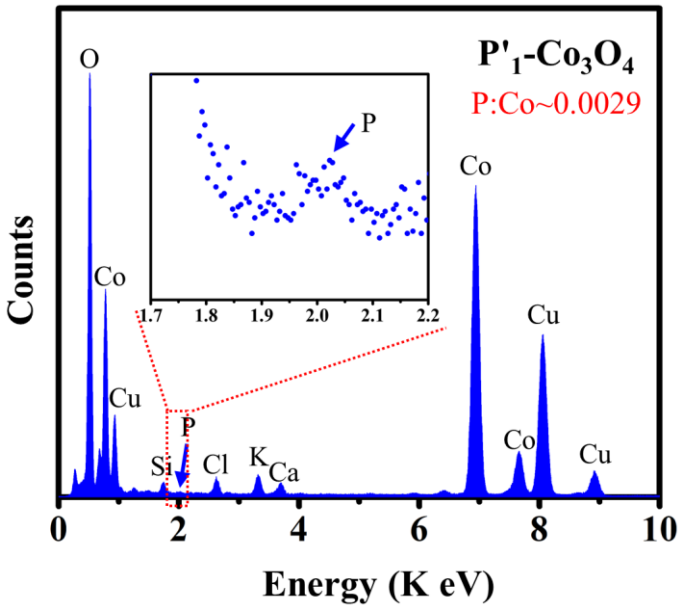

Supplementary Figure 15: The EDX spectrum of P'_1-Co_3O_4 thin-film.

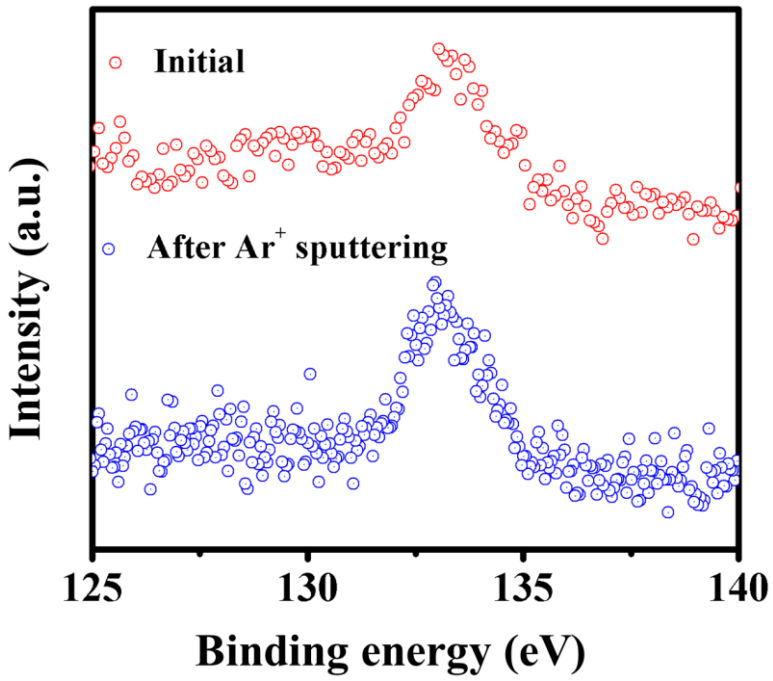

Supplementary Figure 16: High-resolution P 2p spectra before and after Ar^+ sputtering.

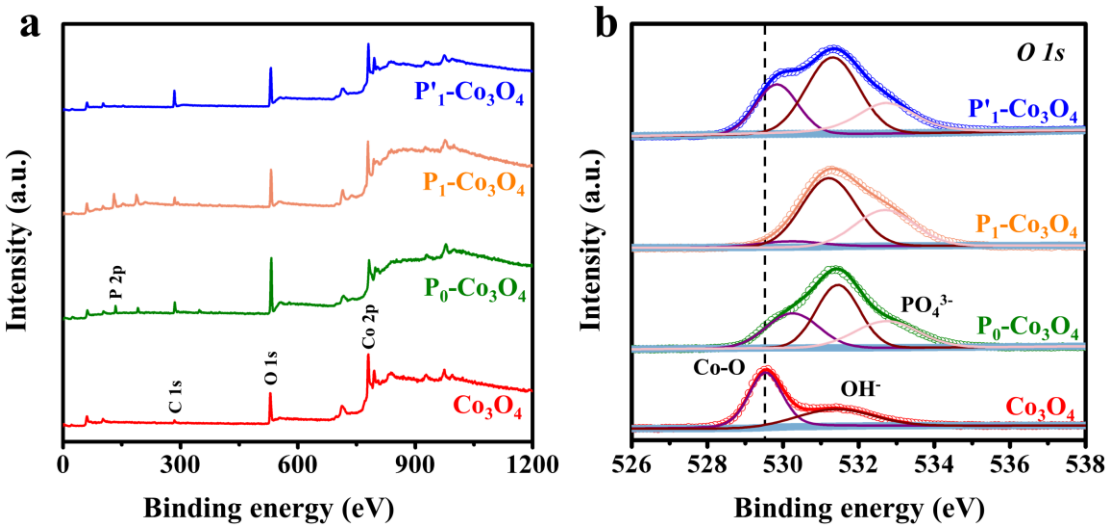

Supplementary Figure 17: High-resolution XPS survey spectra **(a)** and O 1s spectra **(b)** for Co_3O_4, P_0-Co_3O_4, P_1-Co_3O_4 and P'_1-Co_3O_4 thin-films. In O 1s spectra, the peak located at 531.44 eV is related to the presence of surface OH groups.[3] When converting Co_3O_4 into P_0-Co_3O_4, P_1-Co_3O_4 or P'_1-Co_3O_4, the intensity of OH peak becomes higher due to the existence of $H_2PO_4^-$, in which also contains the OH groups. New peaks have appeared at 532.74 eV for P_0-Co_3O_4, P_1-Co_3O_4 and P'_1-Co_3O_4, which is ascribed to PO_4^{3-}.[4] Notably, in comparison with Co_3O_4, Co-O peaks exhibit higher binding energy in P_0-Co_3O_4, P_1-Co_3O_4 and P'_1-Co_3O_4, suggesting the electronic coupling between Co-O bonds and P-O bonds.

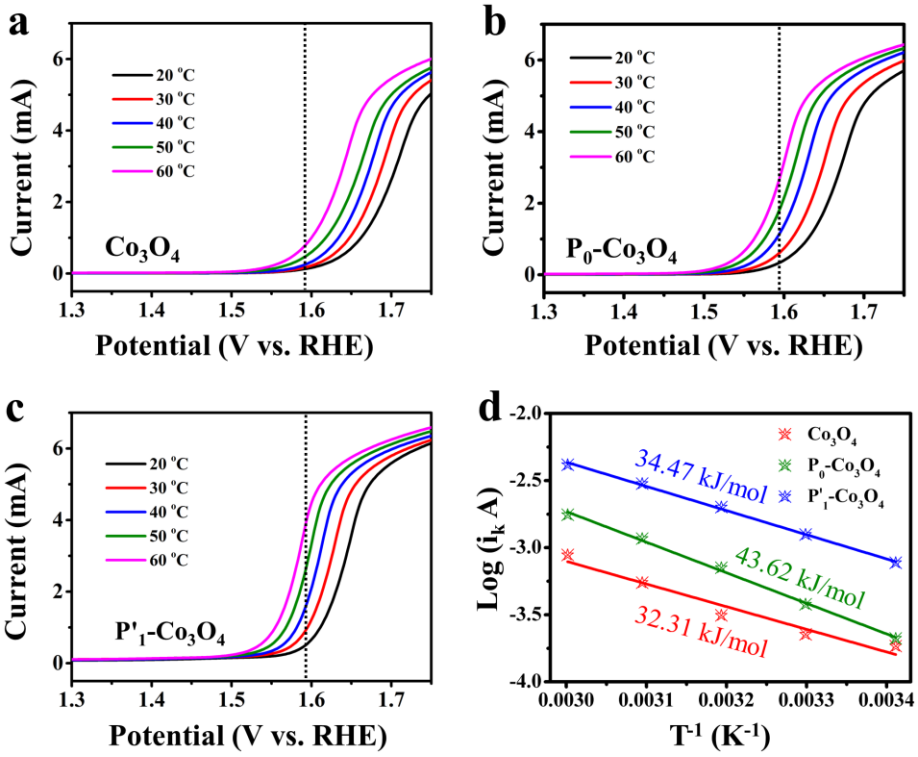

Supplementary Figure 18: LSV curves of 5 mV s^{-1} at different temperatures from 20 to 60 °C for Co_3O_4 **(a)** P_0-Co_3O_4 **(b)** and P'_1-Co_3O_4 **(c)**. **(d)** Arrhenius plots of the kinetic currents at 1.58 V (vs RHE) for Co_3O_4, P_0-Co_3O_4 and P'_1-Co_3O_4, respectively.

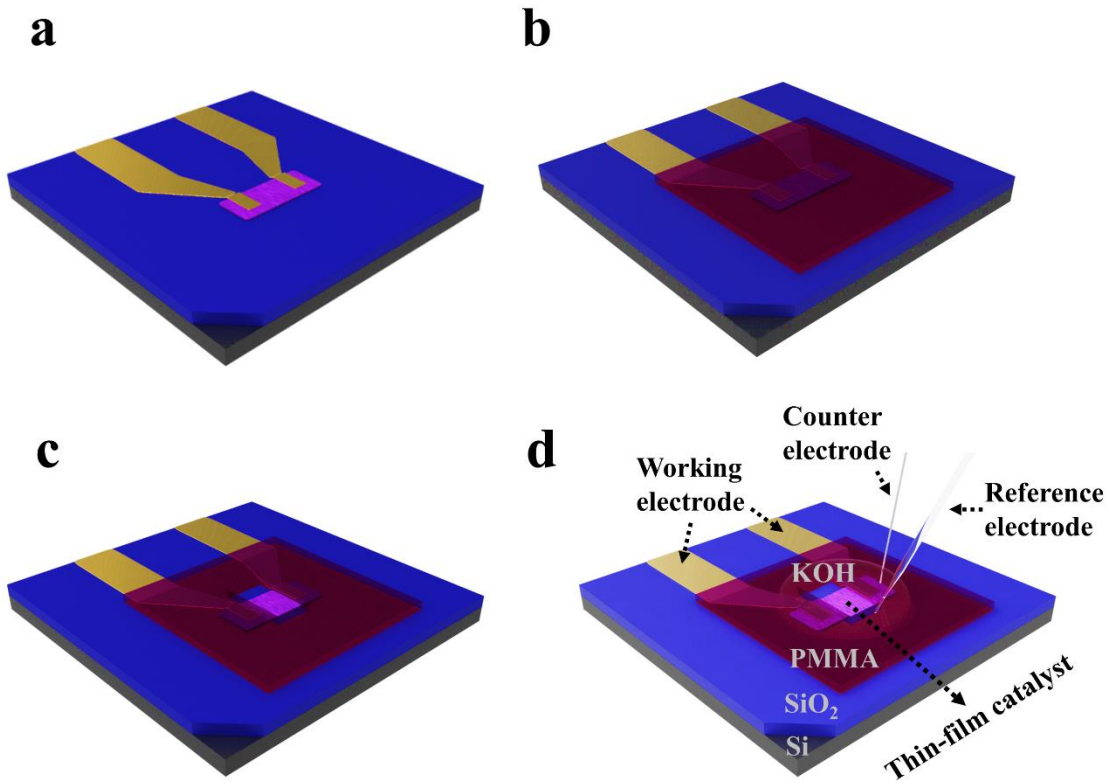

Supplementary Figure 19: The microfabrication of the planar electrochemical device based on already prepared two-terminal thin-film devices. **(a-d)** The schematic diagram of the fabricated procedure.

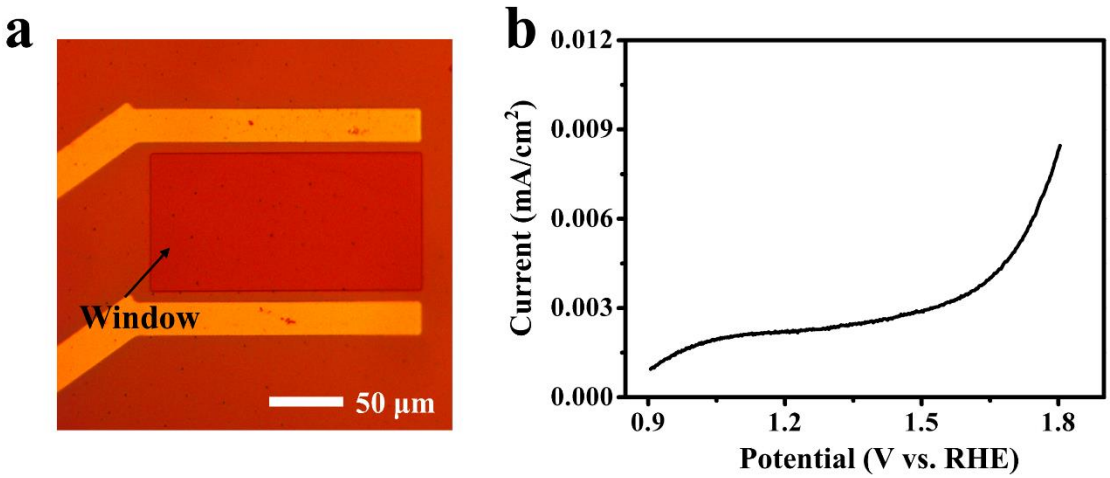

Supplementary Figure 20: (a) The optical image and **(b)** corresponding LSV curve of blank device.

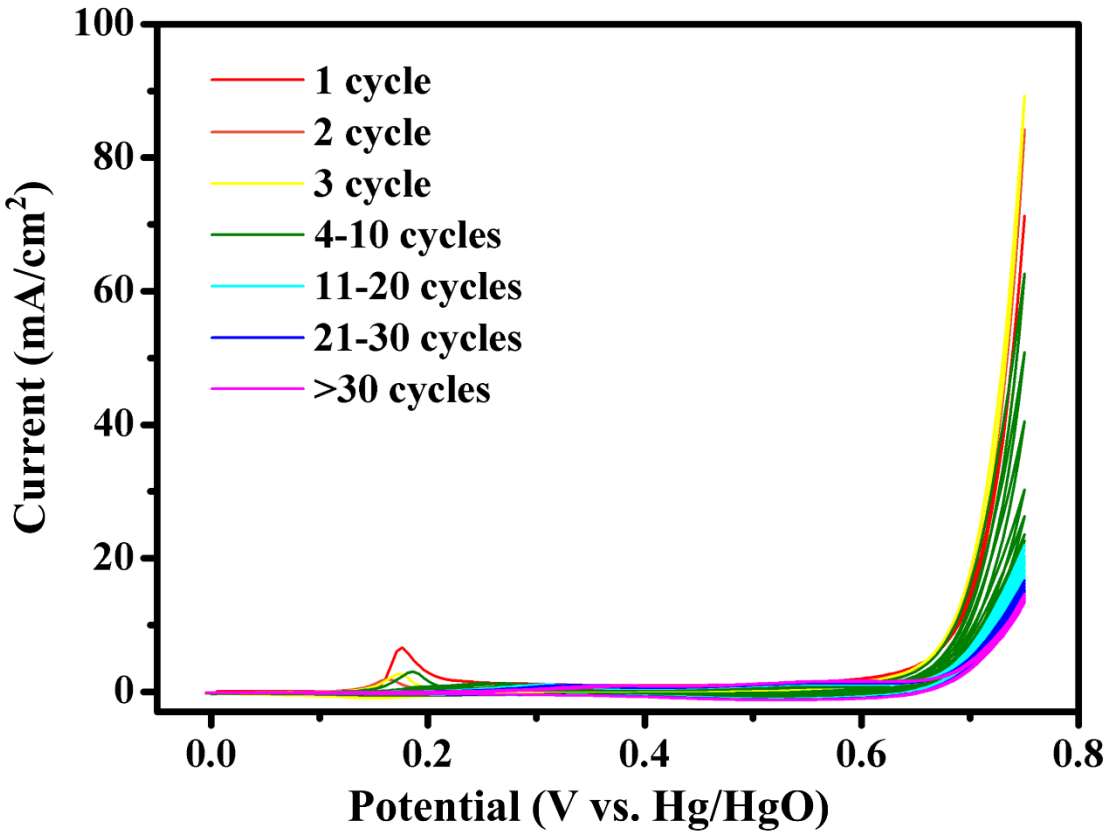

Supplementary Figure 21: Initial 50 cycles CV curves of P_1-Co_3O_4.

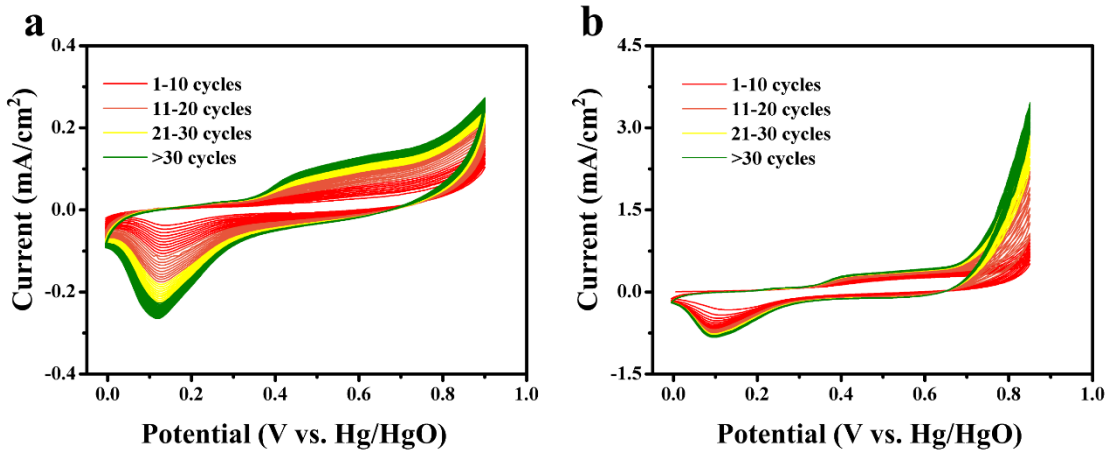

Supplementary Figure 22: Initial electrochemical CV curves of Co_3O_4 **(a)** and P_0-Co_3O_4 **(b)**.

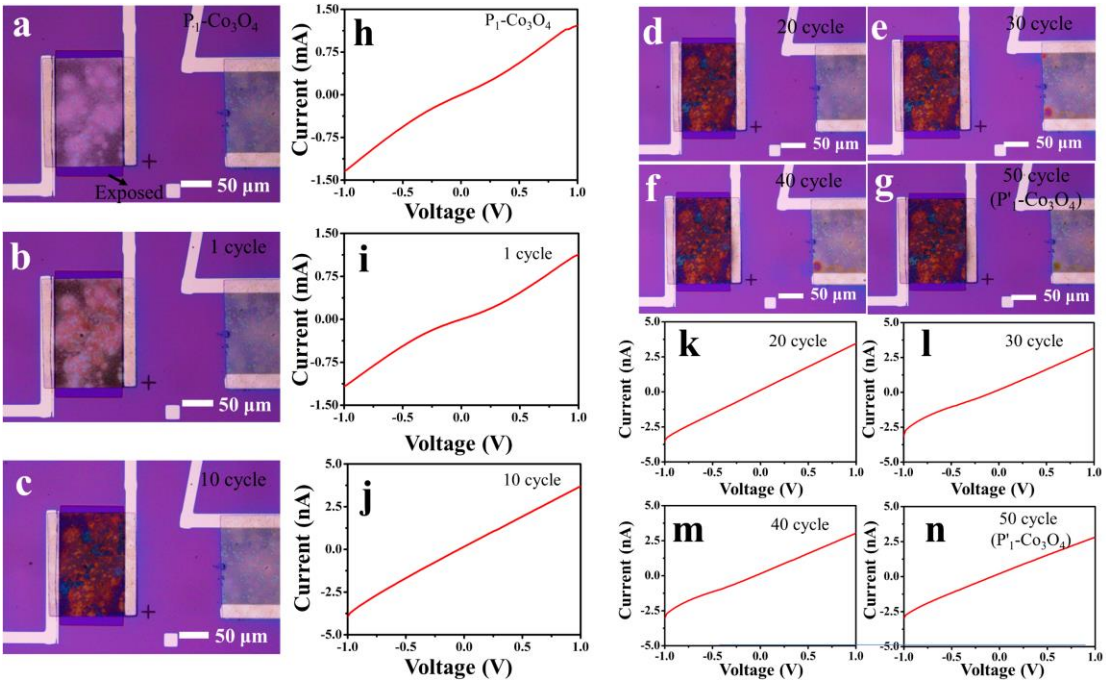

Supplementary Figure 23: (a-g) Optical micrographs of the planar electrochemical microdevice based on individual P_1-Co_3O_4 thin-film after different electrochemical cycles, and **(h-n)** the corresponding *I-V* curves. There are obvious differences in optical images and *I-V* curves from 1st to 10th cycle, indicating a drastic change in the crystal structure of P_1-Co_3O_4.

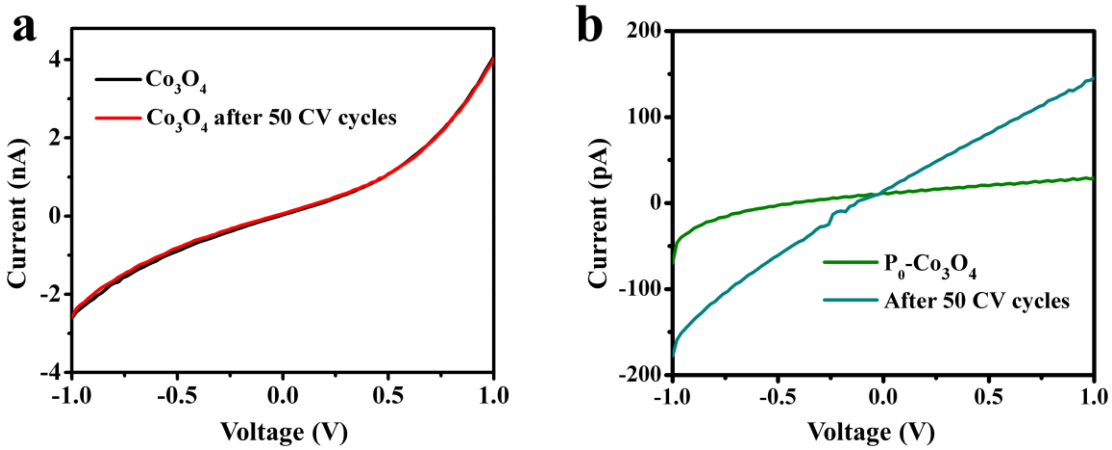

Supplementary Figure 24: The *I-V* curves of Co_3O_4 (a) and P_0-Co_3O_4 (b) thin-films before and after 50 electrochemical CV cycles.

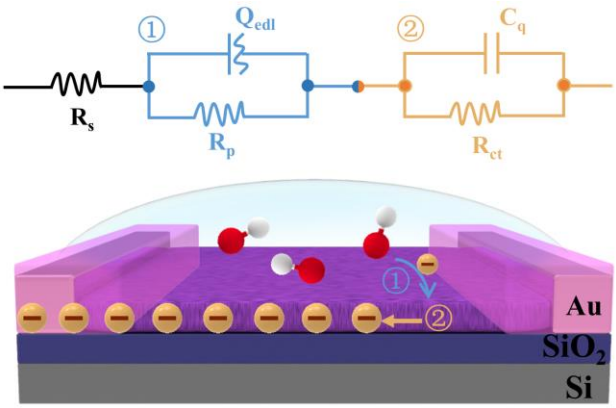

Supplementary Figure 25: Equivalent Randles circuit of individual thin-film-based OER microdevices, in which electrons transfer mainly go through two steps.[5] During process ①, the electrons transfer from OH^- to electrocatalytic interface. R_p is the Faradaic charge-transport resistance and Q_{edl} is related to the EDL capacitance at the electrocatalytic interface. During process ②, the electrons transfer in the thin-film electrode and reach to Au electrodes. R_{ct} and C_q refer to the charge transfer resistance in the thin-film and quantum capacitance, respectively. In addition, the uncompensated electrolyte resistance (R_s) in the experiment is very small which can be ignored.

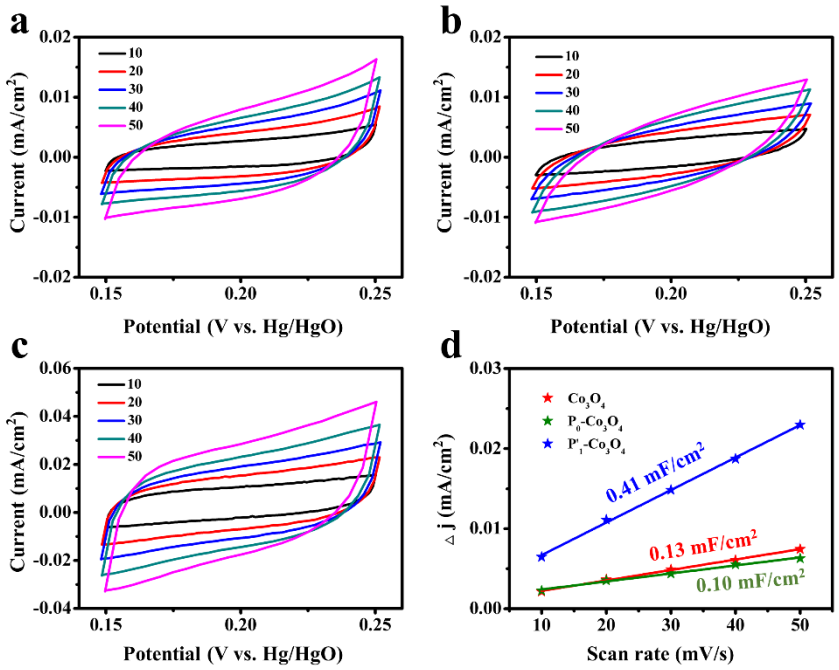

Supplementary Figure 26: Cyclic voltammogram curves of Co_3O_4 (a), P_0-Co_3O_4 (b) and P'_1-Co_3O_4 (c) at different scan rates: 10, 20, 30, 40, and 50 mV s^{-1} in 1.0 M KOH. (d) Corresponding capacitive currents at 0.20 V vs. Hg/HgO as a function of scan rates for Co_3O_4, P_0-Co_3O_4 and P'_1-Co_3O_4.

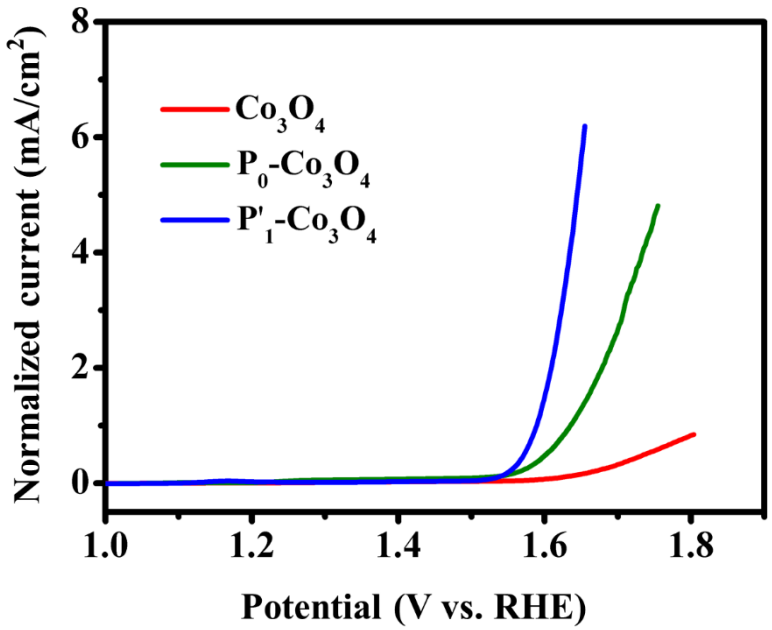

Supplementary Figure 27: The normalized LSV curves of Co_3O_4, P_0-Co_3O_4 and P'_1-Co_3O_4.

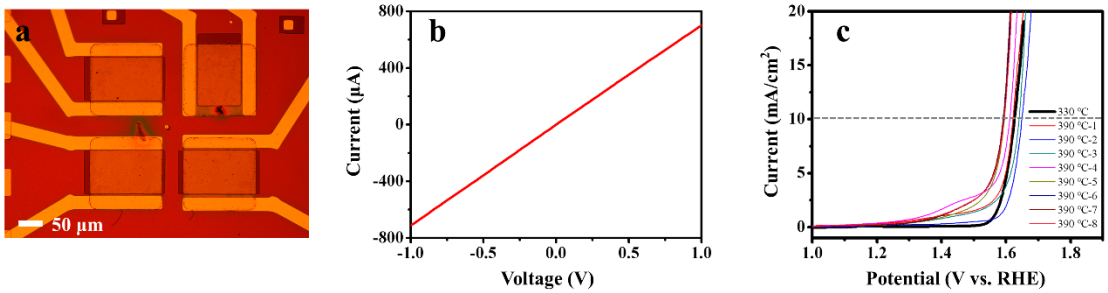

Supplementary Figure 28: The optical image (a) and I-V curve (b) of unreacted P_1-Co_3O_4 (390 ℃) thin-film based OER microdevice. (c) Polarization curves from multiple P'_1-Co_3O_4 (390 ℃) thin-film based OER microdevices, compared with P'_1-Co_3O_4 (330 ℃) thin-film based OER microdevice ("330 ℃" and "390 ℃" refer to the phosphating temperature).

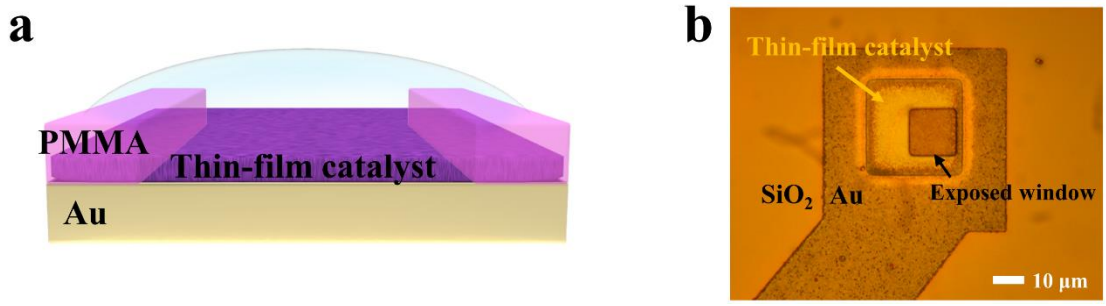

Supplementary Figure 29 (a) The electrochemical set-up for electrocatalytic OER measurements, in which the thin-films were placed on Au substrate. The fabricated process was similar to supplementary Figure 12, we deposited the individual thin-film on the Au outer electrodes but not SiO_2 substrate **(b)** The corresponding optical image of the microdevice based on individual thin-film catalyst.

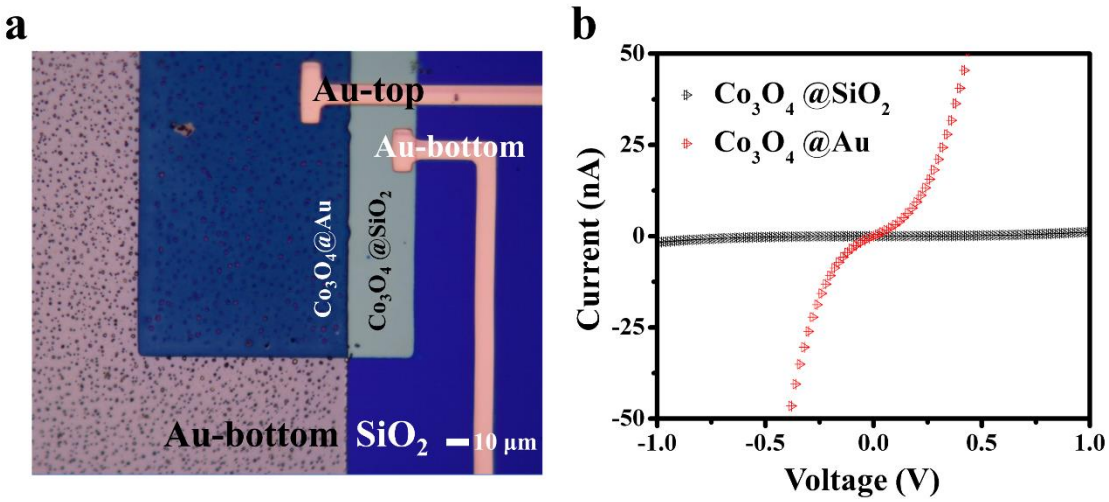

Supplementary Figure 30: (a) The optical image of the device, in which the Co_3O_4 thin-films was partially deposited on Au substrate and SiO_2 substrate. **(b)** The *I-V* curves of the Co_3O_4 @SiO_2 and Co_3O_4 @Au substrate.

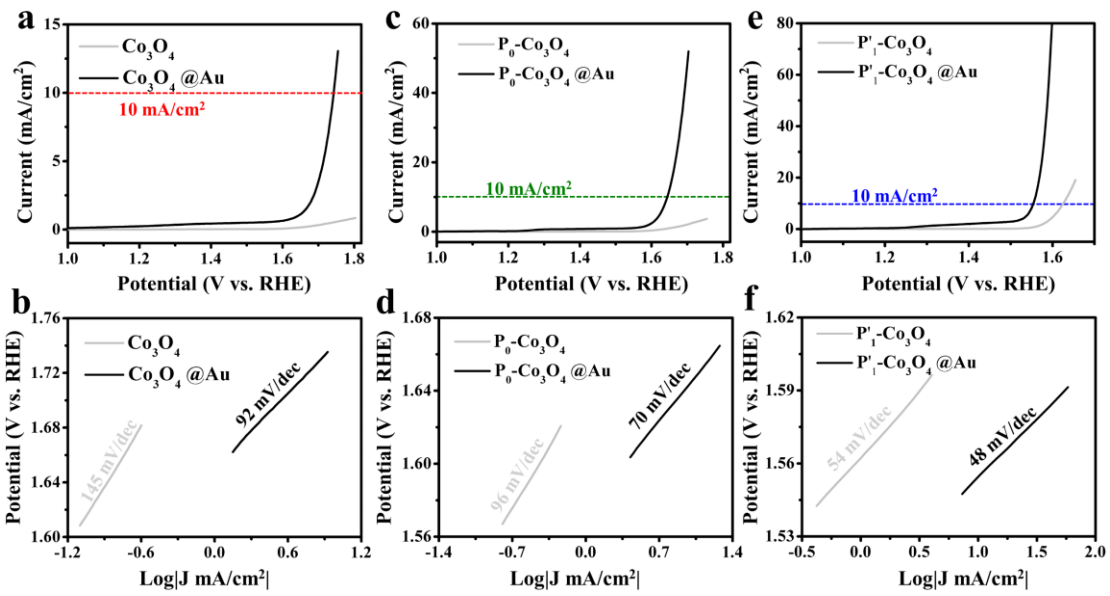

Supplementary Figure 31: The LSV plots and Tafel slopes of Co_3O_4 **(a-b)**, P_0-Co_3O_4 **(c-d)** and P'_1-Co_3O_4 **(e-f)** thin-films with or without Au substrate.

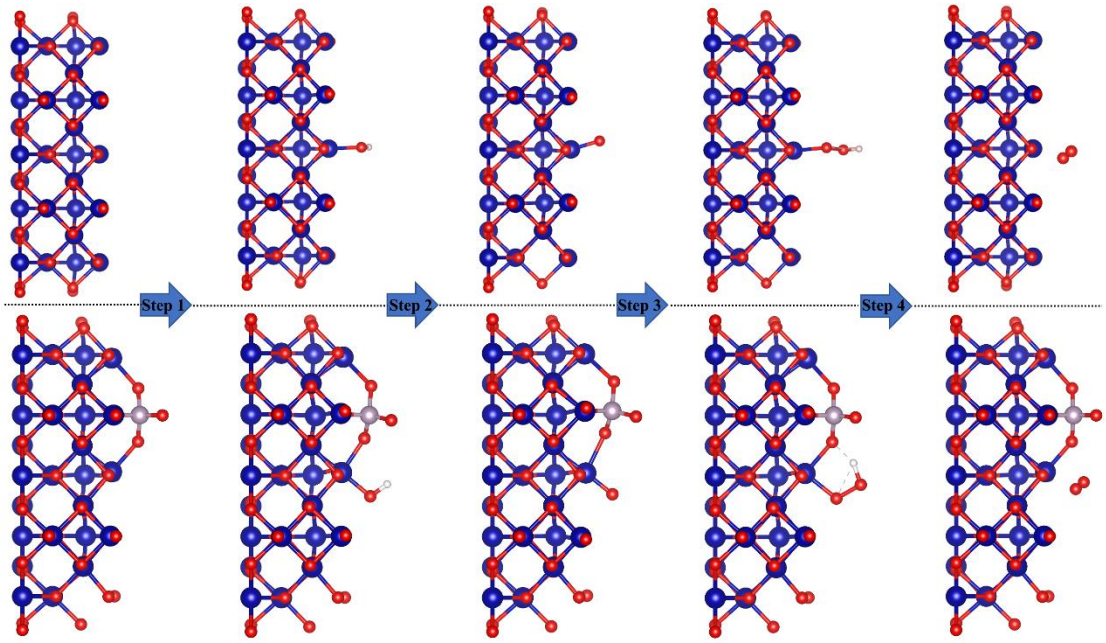

Supplementary Figure 32: the theoretical structures of Co_3O_4 (top) and P'_1-Co_3O_4 (bottom) with intermediates adsorbed during OER process. Blue, red, gray and white spheres represent Co, O, P and H atoms, respectively. The four-steps in an alkaline environment for the OER process are as follows:

$$OH^- + * \longrightarrow *OH + e^- \text{ (step 1)}$$

$$*OH + OH^- \longrightarrow *O + H_2O + e^- \text{ (step 2)}$$

$$*O + OH^- \longrightarrow *OOH + e^- \text{ (step 3)}$$

$$*OOH + OH^- \longrightarrow O_2 + H_2O + e^- \text{ (step 4)}$$

Where * represents the active sites. *OH, *O and *OOH are the adsorbed intermediates during the OER.

References in supporting information

[1] M. Wang, C.-L. Dong, Y.-C. Huang, Y. Li, S. Shen, *Small*, *14* (**2018**) 1801756.

[2] Z. Wang, H. Liu, R. Ge, X. Ren, J. Ren, D. Yang, L. Zhang, X. Sun, *ACS Catal.*, *8* (**2018**) 2236-2241.

[3] Chao Zhang, Markus Antonietti, T.-P. Fellinger, *Adv. Funct. Mater.*, *24* (**2014**) 7655-7665.

[4] T. Zhai, L. Wan, S. Sun, Q. Chen, J. Sun, Q. Xia, H. Xia, *Adv. Mater.*, *29* (**2016**) 1604167.

[5] Y. He, Q. He, L. Wang, C. Zhu, P. Golani, A.D. Handoko, X. Yu, C. Gao, M. Ding, X. Wang, F. Liu, Q. Zeng, P. Yu, S. Guo, B.I. Yakobson, L. Wang, Z.W. Seh, Z. Zhang, M. Wu, Q.J. Wang, H. Zhang, Z. Liu, *Nat. Mater.*, *18* (**2019**) 1098-1104.